Orientational Order of the Polyene Fatty Acid Membrane Probe *trans*-Parinaric Acid in Langmuir−Blodgett Multilayer Films

S. Lopes,[†,‡] M. X. Fernandes,[‡] M. Prieto,[†] and M. A. R. B. Castanho*[,†,‡]

Centro de Química-Física Molecular, Instituto Superior Técnico, Av. Rovisco Pais, 1049-001 Lisboa, Portugal, and Departamento de Química e Bioquímica da Faculdade de Ciências da Universidade de Lisboa, Campo Grande, Ed. C8 - 6° Piso, 1749-016 Lisboa, Portugal

Received: July 26, 2000

trans-Parinaric acid, a polyene fatty acid, is widely used as a fluorescent membrane probe in photophysical and biophysical studies. We have worked on the orientational order of this molecule in Langmuir−Blodgett multilayer films of both gel-phase dipalmitoylphosphatidylcholine and arachidic acid at room temperature. Namely, orientational density probability functions were calculated using the maximum entropy method. Because liquid-crystal lipids do not deposit forming multilayers by Langmuir−Blodgett techniques, we have used Brownian dynamics methods to simulate a *trans*-parinaric acid molecule in a liquid-crystal bilayer environment. Orientational density probability functions are also achieved under the ergodic hypothesis. In the gel phase, *trans*-parinaric acid is highly ordered (narrow density probability function) and almost perpendicular (78°) to the multilayer planes. In the liquid-crystal phase, the density probability function broadens and the average orientation is not so close to the multilayer normal axis. The highly ordered system detected in the gel phase is in agreement with the preference for the gel phase in the partitioning of this probe among different phases, which is a very peculiar behavior. If its inclusion was not a favorable process, i.e., not adjusted to the membrane geometry, it could not have such a strict alignment. The change in orientational distribution upon phase transition is in agreement with published data on the dynamics of the probe in the nanosecond time range.

Introduction

trans-Parinaric acid (*t*-PnA; Figure 1) has long been used as a membrane probe.[1] Its polyene chromophore does not have the disadvantage of bulky probes and is very well studied from the photophysical point of view.[2] Despite an intrinsically complex fluorescence decay,[3] most UV−vis spectroscopic features are simple and known. For instance, the relative orientations of the transition moment and the molecular axis have been established, and the angle between the two is only 15°.[4] This close collinearity makes *t*-PnA a potential molecule to be studied by linear dichroism techniques because no critical correction for this effect is needed. Although *t*-PnA is a very common membrane probe, information on its orientation is lacking, to our best knowledge. The information aimed in the present work is relevant for the study of the interactions between lipid membranes and fatty acids. Whereas Langmuir−Blodgett (LB) films consisting of multilayers of gel-phase lipids can be prepared with some simplicity, liquid-crystal phase lipids cannot be used for deposition.[5] Thus, to overcome this difficulty and maintain our goal, we have used the powerful tool of Brownian dynamics (BD) to simulate the dynamics of a single *t*-PnA molecule. Under the ergodic hypothesis, this function is also valid for the population ensemble average (population of independent molecules). In the present work, three different classes of multilayers will be used: 1,2-dipalmitoyl-3-*sn*-phosphatidylcholine (DPPC) in the gel phase (room temperature), arachidic acid (AA; room temperature), and a simulated liquid-crystalline environment.

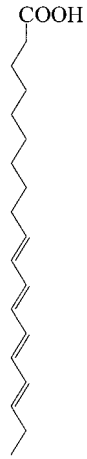

Figure 1. *t*-PnA.

Materials and Methods

LB films were prepared with a NIMA (Coventry, U.K.) trough in a classical fashion. A 10 μL sample of DPPC or a 25 μL sample of AA solutions in chloroform (1 mg/ml) was placed in the surface of the subphase (Millipore water for DPPC and 1 mM $Pb(NO_3)_2$ for AA) and left to evaporate the chloroform for 1 h. Depositions were carried out over 1 mm thick quartz plates specially prepared by Precision Glass & Optics (Santa Ana, CA) at surface pressures of 40 mN/m for DPPC and 30 mN/m for AA. Three layers of DPPC on each side of the plate were obtained in some depositions, with typical transfer efficiencies of 80%. Selected samples with DPPC and *t*-PnA had three layers on each side. The number of layers in the blank was not relevant because it did not affect the results (zero to

* To whom correspondence should be addressed. E-mail: pcmcastanho@popsrv.ist.utl.pt. Fax: 351 21 8464455.
† Instituto Superior Téchnico.
‡ Universidade de Lisboa.

10.1021/jp0026742 CCC: $20.00
Published on Web 12/22/2000

three layers). Samples with AA were used with at least 11 layers on each side of the quartz plate, and blank subtraction was also carried out. The topological quality of the samples was assessed by atomic force microscopy (data not shown; courtesy of Dr. Luís de Melo, Instituto Superior Técnico, Lisboa, Portugal) with a Microscope from Digital Instruments (Santa Barbara, CA).

UV−vis absorption measurements were carried out in a Shimadzu spectrophotometer (model UV-3101 PC), having a reported repeatability of ±0.001. Dichroic ratios were determined using Glan−Thompson polarizers in homemade stands. Blank correction was carried out by reading both sample and blank (pure DPPC or pure AA films) against air and subtracting afterward. The quartz plates were mounted in a goniometer (Optosigma; Santa Ana, CA), which replaced the usual sample holder. The whole experimental setup was tested by preparing multilayers of DPPC with cyanine dyes. The average orientation angles reported in the literature for these test probes were reproduced.[6] A spectrofluorimeter (SLM-Aminco 8100), equipped with a 450 W Xe lamp and double monochromators in both excitation and emission, as well as a quantum counter was also used. The polarizers and goniometer were the ones mentioned earlier.

Dichroic ratios and fluorescence intensity ratios were measured in the ranges 0−72° and 18°−72°. respectively. Excitation and emission wavelengths were respectively 323 and 410 nm (AA) or 319 and 410 nm (DPPC). An optical cutoff filter was used before the excitation polarizer to reduce stray light.

Theoretical Background and Data Analysis. Data analysis methodologies are generally described in ref 7. For cylindrically symmetric molecules, the orientation distribution is described by the single particle function $f(\psi)$, where ψ is the angle between the long axis of a molecule and the director of the system (normal to the multilayer plane)

$$f(\psi) = \sum_{L=\text{even}} \frac{1}{2}(2L+1)\langle P_L\rangle P_L(\cos\psi) \tag{1}$$

P_L is the Legendre polynomial of the Lth order and $\langle P_L\rangle$ is the ensemble average of $P_L(\cos\psi)$ and is called the Lth rank order parameter. The density probability function associated to ψ is $\sin(\psi)\, f(\psi)$, and so

$$\int_0^{\pi} \sin(\psi)\, f(\psi) = 1 \tag{2}$$

Only $\langle P_2\rangle$ and $\langle P_4\rangle$ are experimentally accessible, but truncation of eq 1 for the two first terms may lead to a rather poor approximate description of $f(\psi)$. One way to overcome this problem combines the application of maximum entropy method with the formalism of the Lagrange multipliers method.[8] In practice, one seeks the values of the constants λ_2 and λ_4 that satisfy eqs 3−5

$$\langle P_2\rangle = \int_0^{\pi} \sin\psi P_2(\cos\psi)\, f(\psi)\, \mathrm{d}\psi \tag{3}$$

$$\langle P_4\rangle = \int_0^{\pi} \sin\psi P_4(\cos\psi)\, f(\psi)\, \mathrm{d}\psi \tag{4}$$

$$f(\psi) = \frac{\exp(\lambda_2 P_2(\cos\psi) + \lambda_4 P_4(\cos\psi))}{\int_0^{\pi} \sin\psi \exp(\lambda_2 P_2(\cos\psi) + \lambda_4 P_4(\cos\psi))\, \mathrm{d}\psi} \tag{5}$$

$f(\psi)$ calculated this way represents the broadest distribution possible that is compatible with the experimentally determined values of $\langle P_2\rangle$ and $\langle P_4\rangle$. λ_2 and λ_4 were determined by a least-squares method where the (λ_2, λ_4) space was searched for the best solution of eqs 3 and 4. The (λ_2, λ_4) solutions lead the two members in eqs 3 and 4 to be identical with a maximum error of 3.9×10^{-5}% relative to $\langle P_2\rangle$ and $\langle P_4\rangle$ simultaneously, in all of the studied systems.

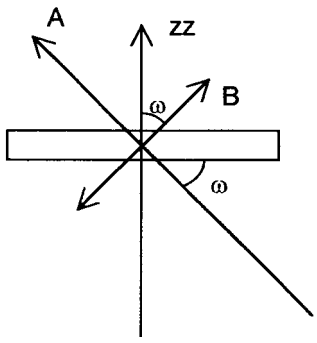

Figure 2. Experimental setup for the $\langle P_2\rangle$ calculation with UV−vis absorption measurements. The zz axis is the system director, A is the incident beam, and B is the polarization direction.

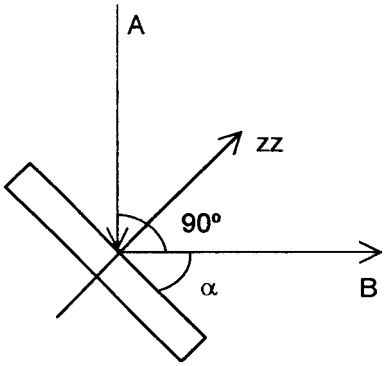

Figure 3. Experimental setup for the $\langle P_4\rangle$ calculation with steady-state fluorescence measurements. The zz axis is the system director and A and B are the directions of excitation and detection, respectively.

$\langle P_2\rangle$ was calculated using the setup depicted in Figure 2 and eq 6. Inclusion of the sin ω term accounts for the increasing area of the illuminated sample as ω decreases. An alternative to this procedure is to perform a measurement with vertical polarized light instead of $A_{\omega=\pi/2}$.[9] $\langle P_4\rangle$ was calculated as proposed by Kooyman et al.,[7] i.e., by means of steady-state fluorescence spectroscopy (eq 7) having excitation and emission in a 90° angle geometry (Figure 3). The strong collision model framework[7] was adopted. A single correlation time, τ_0, is present, which can be interpreted as the time during which the transition moment has a particular, fixed orientation relative to the director (eq 11). Under the assumption that $\langle P_2\rangle$ and w are the same in ordered (e.g., LB films) and disordered (e.g., vesicles) samples, eq 12 holds, where r is the steady-state fluorescence anisotropy. r values for t-PnA are available in the literature[3,10] for lipid bilayers. The value for AA multilayers was assumed to be identical. This is a reasonable approximation because r does not severely depend on the host matrix acyl chain length.[3]

$$\frac{\sin(\omega)A_{\omega}}{A_{\omega=\pi/2}} = 1 + \frac{3\langle P_2\rangle}{(1-\langle P_2\rangle)n^2}\cos^2\omega \tag{6}$$

A_{ω} is the absorbance at angle ω, and n is the relative refraction index, equal to 1.5.[7]

$$I_{\text{vh}}/I_{\text{vv}} = a\sin^2\alpha + b \tag{7}$$

α is the angle depicted in Figure 3. The first and second

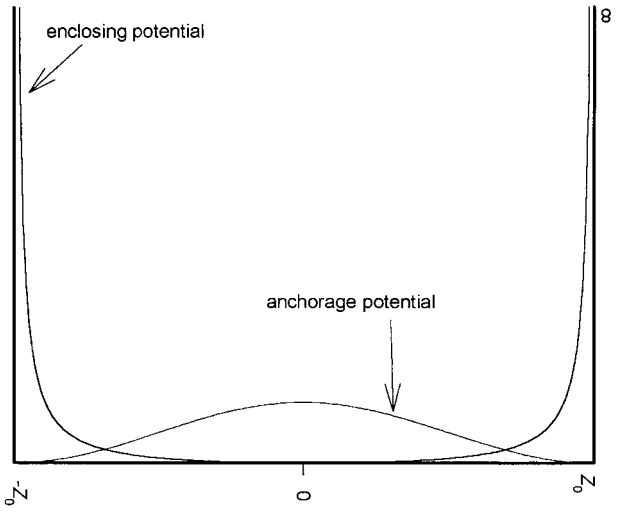

Figure 4. Profile of mean field potentials in the phospholipid bilayer.

subscripts refer to the excitation and emission polarizers orientation, respectively (v - vertical, h - horizontal).

$$a = \frac{\left(\frac{3}{7}\langle P_4\rangle + \frac{4}{7}\langle P_2\rangle - \langle P_2\rangle^2\right)w + \langle P_2\rangle^2 - \langle P_2\rangle}{c} \quad (8)$$

$$b = \frac{1}{3}\frac{1 - \left(\frac{2}{5} + \frac{36}{35}\langle P_4\rangle + \frac{4}{7}\langle P_2\rangle - 2\langle P_2\rangle^2\right)w - 2\langle P_2\rangle^2 + \langle P_2\rangle}{c} \quad (9)$$

$$c = \frac{1}{3}\left[1 + \left(\frac{4}{5} - \frac{4}{7}\langle P_2\rangle + \frac{27}{35}\langle P_4\rangle - \langle P_2\rangle^2\right)w + \langle P_2\rangle^2 - 2\langle P_2\rangle\right] \quad (10)$$

$$w = \frac{\tau_0}{\tau_0 + \tau} \quad (11)$$

$$r = \frac{2}{5}[\langle P_2\rangle^2 + w(1 - \langle P_2\rangle^2)] \quad (12)$$

Correction Factors

The correction factors were dealt with in detail by Kooyman et al.[7] Two significant factors should be taken into account: (1) the angular-dependent propagation of light passing through an interface of two isotropic media having different refraction indices and (2) the transmission fraction of light passing through a boundary of two media which is dependent on its polarization state. The first factor is corrected by Snell's law, whereas the second is corrected by means of Fresnel's law; corrections were made accordingly. Blank subtraction was always carried out. I_{vh}/I_{vv} (eq 7) was corrected by the geometry factor G ($= I_{hv}/I_{hh}$), to account for different transmittances of the emission monochromator for vertically and horizontally polarized light. G, an instrumental factor, was determined in a homogeneous solution for better accuracy.

BD Simulation

We performed a BD simulation of a *t*-PnA molecule with atomic level detail, using the extended atom representation, meaning that hydrogen atoms are not explicitly represented. In this way, we can get precise information about the structure and dynamics of a molecule because BD allow us to span all of the available conformational space and to produce long time trajectories, which give a more meaningful picture of processes that occur in membranes.

TABLE 1: Parameters for the Simulation of the Hydrocarbon Chain's Internal Energy[a]

Lennard-Jones Potential	
parameter	magnitude
σ	3.92 Å
ϵ	600×10^6 kJ/mol
Torsional Potential	
parameter (sp^3-sp^3)	magnitude (kJ/mol)
c_0	8.113
c_1	15.591
c_2	−4.476
c_3	−15.478
c_4	8.951
c_5	−12.681
parameter (sp^3-sp^2)	magnitude (kJ/mol)
c_1	−3.568
c_2	−0.462
c_3	9.696
parameter (sp^2-sp^2)	magnitude (kJ/mol)
k_ϕ	3600
Bending Potential	
parameter (sp^3)	magnitude
bond angle	111°
bending constant	520 kJ/mol
parameter (sp^2)	magnitude
bond angle	120°
bending constant	1040 kJ/mol
Stretching Potential	
parameter	magnitude
sp^3-sp^3 bond length	1.53 Å
stretching constant	1.044×10^3 kJ/(mol Å^2)
sp^3-sp^2 bond length	1.51 Å
stretching constant	1.044×10^3 kJ/(mol Å^2)
sp^3-sp^2 bond length	1.32 Å
stretching constant	1.044×10^3 kJ/(mol Å^2)

[a] Stretching potential constants, ref 30; other parameters, ref 11.

Model, Energetics, and Simulation Method. The system that we simulate consists of a molecule with 18 friction elements moving in the environment of a phospholipid bilayer of a given thickness. The simulated molecule reproduces the geometry and dimension of the *t*-PnA chain, which has 18 carbon atoms and 4 conjugated double bonds. The methyl and methylene groups are represented by spheres joined by a frictionless connector, with one extremity sphere (a pseudoatom that represents the carboxyl group) tending to be anchored to the membrane interface. None of the spheres of our simulated chains can trespass the $|z_0|$ planes of the membrane, as depicted in Figure 4, meaning that the chain trajectories are confined to the membrane interior.

Hydrocarbon Chain Energetics. The total intramolecular potential considered has contributions resulting from stretching potential, bending potential, torsional potential, and nonbonded pairwise interaction potential, and their magnitudes are listed in Table 1.

First we will consider the potentials applied to the hydrocarbon backbone. The stretching potential is defined by a harmonic potential that maintains the equilibrium bond length of carbon−carbon bonds and has the following expression:

$$V_s = 0.5K_s(d_i - d_i^0)^2 \quad (13)$$

where K_s is the spring constant, d_i is the instantaneous distance between i ($i = 1, ..., 17$) and $i + 1$, and d_i^0 is the equilibrium distance between i and $i + 1$. This equilibrium distance is different according to the C atoms involved in the bond.[11] For a sp^3-sp^3 bond, d_i^0 is 1.53 Å; for a sp^2-sp^3 bond, d_i^0 is 1.51 Å; and for a sp^2-sp^2 bond, d_i^0 is 1.32 Å.

The bending potential, which is similar to the stretching potential, is of a harmonic type. Its expression is

$$V_b = 0.5K_b(\alpha'_i - \alpha_0)^2 \quad (14)$$

where K_b is the bending constant, α'_i ($i = 1, ..., 16$) is the instantaneous bending angle, and α_0 is the equilibrium bending angle. Once again the equilibrium angle is different according to the type of C atom involved,[11] meaning that α_0 is 111° if the C atom is sp^3 and α_0 is 120° if the atom is sp^2.

The torsional potential is given by the following expression:[12]

$$V_\phi = \sum_{k=0}^{5} c_k(\cos \phi_i)^k \quad (15)$$

if both C atoms that bracket the bond, whose rotation is considered, are sp^3. If one of the C atoms is sp^3 and the other is sp^2, the torsional potential expression becomes[11]

$$V_\phi = c_1(1 + \cos(\phi)) + c_2(1 - \cos(2\phi)) + c_3(1 + \cos(3\phi)) \quad (16)$$

If the C atoms are both sp^2, the rotation around the double bond is avoided using the potential expression[11]

$$V_\phi = k_\phi(\cos \phi - \cos \phi_0)^2 \quad (17)$$

where, in all of the torsional potential expressions, ϕ_i is a dihedral angle ($i = 1, ..., 15$) and $\phi_0 = 0°$, because all double bonds are in the trans conformation ($\phi = 120°$and $\phi = -120°$ for gauche(+) and gauche(−) conformations, respectively).

The interaction potential for nonbonded atoms, applied to every single atom, is described by the Lennard-Jones potential:

$$V_{LJ} = 4\epsilon\left(\left(\frac{\sigma}{r_{ij}}\right)^{12} - \left(\frac{\sigma}{r_{ij}}\right)^{6}\right) \quad (18)$$

where r_{ij} is the distance between atoms i and j, ϵ is the depth of the potential, and σ is the distance where the Lennard-Jones potential is zero. The magnitudes for all potential constants are listed in Table 1.

Membrane Energetics. We use a hard-wall potential to confine the motion of simulated molecules to the interior of our model membrane. This potential acts whenever a sphere of the simulated hydrocarbon chains leaves the allowed region of motion, and its effect is to place the mentioned sphere once again inside the model membrane. The confinement of the chain elements to the desired region is represented by the following:

$$\begin{cases} V_{conf} = 0 & \text{if } |z| \le z_0 \\ V_{conf} = \infty & \text{if } |z| > z_0 \end{cases} \quad (19)$$

To describe the membrane environment, we considered three distinct potentials. The first one takes into account the nonpolarity of the methyl and methylene groups, and their interaction with the finite model membrane along the z direction, and has the form of[13]

$$V_{encl}(z_i) = \frac{kTK_z}{z_0^2 - z_i^2} \quad (20)$$

where i runs from 2 to 18. z_i is the z coordinate of the ith sphere of the chain, z_0 is the half-width of the membrane, k is the Boltzmann constant, T is the temperature, and K_z is the magnitude of the enclosing potential. This potential replicates in a smooth way the behavior of the hard-wall potential. We use this potential mainly to avoid triggering the hard-wall potential, because discontinuities are not desirable. In this way, and generally, the hard-wall potential only acts upon sphere 1 (the one that represents the carboxyl group) of the simulated chains.

The first sphere of the chain was designed to anchor to the membrane boundaries, so it is submitted to an anchorage potential having the expression[14]

$$V_{anch} = kTK_{anch}\cos^2\left(\frac{z_1\pi}{2z_0}\right) \quad (21)$$

where z_1 is the z coordinate of the first sphere of the chain and K_{anch} is the magnitude of the potential. This potential allows a restricted perpendicular motion of the entire hydrocarbon chain.

To simulate the ordering effect induced by the membrane environment, a Maier−Saupe potential is introduced. This potential pushes the simulated chain to a more parallel orientation to the transverse plane of the membrane, that is to say, along the z axis. The field strength, K_θ, of this potential is not constant throughout the membrane, reproducing the different packing of hydrocarbon tails in biological membranes determined by neutron diffraction.[15] It changes with linear dependence according to the distance of the membrane boundaries

$$K_\theta(z) = K_\theta^0 + q|z| \quad (22)$$

being higher at the membrane boundaries and lower at the membrane interior. In this way, it is possible to reproduce the deuterium order parameters of a hydrocarbon molecule in a model membrane.[16] The potential is given by

$$V_{orient} = -\frac{3}{2}kTK_\theta(z)\,(\cos^2\theta_i - 1) \quad (23)$$

where $K_\theta(z)$ is the field strength of the orientational potential and θ_i is the angle formed by the z axis and the vector that joins atoms C_{i-1} and C_{i+1}. All of the potentials and their first derivatives, except the hard-wall potential, are continuous within the domain accessible to the motion of the simulated molecule.

Simulation Method. The BD trajectories were simulated using a method based on the algorithm of Ermak and McCammon[17] modified by Iniesta and García de la Torre.[18] Each Brownian step is taken into account twice, in a predictor−corrector way, and the resulting positions of the elements, $\mathbf{r}$, after a time step Δt are obtained from the previous ones, using the following equations:

$$\mathbf{r}' = \mathbf{r}^0 + \frac{\Delta t}{kT}\mathbf{D}^0\cdot\mathbf{F}^0 + \Delta t(\nabla_r\mathbf{D})^0 + \mathbf{R}^0 \quad (24)$$

$$\mathbf{r} = \mathbf{r}^0 + \frac{\Delta t}{kT}\frac{1}{2}(\mathbf{D}^0\cdot\mathbf{F}^0 + \mathbf{D}'\cdot\mathbf{F}') + \Delta t\frac{1}{2}[(\nabla_r\mathbf{D})' + (\nabla_r\mathbf{D})^0] + \mathbf{R}' \quad (25)$$

Equation 24 is used to calculate the predictor substep whose determination is based on quantities corresponding to the initial conformation, $\mathbf{r}^0$. In this substep, an estimate, $\mathbf{r}'$, of the final conformation is obtained and required quantities are evaluated with that conformation. Afterward, the corrector substep is calculated with eq 25, based once again on the initial conformation $\mathbf{r}^0$ but using quantities that arise from the mean of those obtained with conformations $\mathbf{r}^0$ and $\mathbf{r}'$. Although one step in the procedure described here is equivalent to two steps in the Ermak−McCammon algorithm and, consequently, it takes about double the central processing unit (CPU) time of the latter, we can use longer time steps, and there is an increase of efficiency.[18]

The *3N* vectors **r** and **F** are the coordinates and mechanical forces on the *N* beads, and **D** is the $3N \times 3N$ diffusion supermatrix whose *ij* blocks are the diffusion tensors, $\mathbf{D}_{ij}$. $\mathbf{R}^0$ and $\mathbf{R}'$ are random vectors with covariance matrices equal to $2\Delta t\mathbf{D}^0$ and $2\Delta t\mathbf{D}'$, respectively. They are obtained from Gaussianly distributed vectors, with zero mean and unitary variance, $\mathbf{q}$ and $\mathbf{q}'$, as $\mathbf{R}^0 = (2\Delta t)^{1/2}\sigma^0\mathbf{q}$ or $\mathbf{R}' = (2\Delta t)^{1/2}\sigma'\mathbf{q}'$, where σ is a $3N \times 3N$ supermatrix obtained from the square root of **D**.

When dynamic properties were simulated, hydrodynamic interactions (HI) between elements of the system must be adequately taken into account. On the other hand, when equilibrium properties were simulated, HI can be neglected because they do not have any dependence on the rate of dynamic processes. BD without HI are less computationally time-consuming than BD with HI and are the most adequate to span the entire conformational range of simulated molecules. The exclusion of HI is done by setting, for $i \neq j$, $\mathbf{D}_{ij} = 0$ in eq 24. Note that in both cases, HI or no HI, $\mathbf{D}_{ii} = (kT/\xi_i)\mathbf{I}$, where **I** is a unitary 3×3 matrix and ξ_i the friction coefficient of the *i*th spherical element, given by the Stokes law as $\xi_i = 6\pi\eta_0\sigma_i$, with η_0 as the solvent viscosity and σ_i as the radius of the *i*th element.

In the present work, we followed the above strategy, meaning that equilibrium properties were obtained from no HI BD trajectories.

Parametrization of the Simulated System. The parameters for the stretching, bending, torsional, and Lennard-Jones potentials appear in Table 1. The anchorage potential constant, K_{anch}, used was 9.7×10^{-2} kJ/mol; the enclosing potential constant, K_z, takes the value of 19.38 kJ/(mol Å^2), and the orientational potential constant, $K_{q(z)}$, was set to 6.2×10^{-2} kJ/mol at $z = z_0$ and 5.2×10^{-2} kJ/mol at $z = 0$. The potentials were set to these particular values in order to recover the characteristic deuterium order parameter profile and magnitude of a phospholipid and other derived hydrocarbon molecules in a membrane.[14]

The simulations were done with an 18-element chain, with a membrane half-thickness, z_0, of 20 Å,[16] at 315 K just above the phase transition temperature (314 K) of DPPC, with a viscosity of 2.5 cP, with a radius for each friction element of 0.75 Å, with $\Delta t = 4$ fs, and with a total trajectory time of 200 ns. The 30 trajectories thus generated were analyzed to recover equilibrium properties, as averages over the trajectories. We produced the software necessary to generate the simulations in a computer equipped with a Pentium III processor, which took approximately 20 h of CPU time to simulate trajectories.

Results and Discussion

The absorption spectrum of *t*-PnA in planar multilayers is depicted in Figure 5. The measurement angle affects the spectral intensity but not the vibrational progression or the transition energies. Spectral shifts are the ones expected, considering the changes in the polarizability of the surrounding medium.

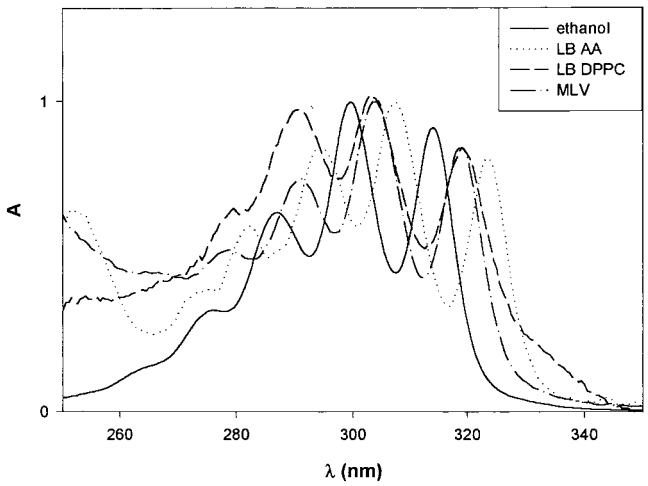

Figure 5. Electronic absorption spectra of *t*-PnA in multilayers of DPPC (− −; $\omega = 72°$), AA (•••; $\omega = 72°$), in aqueous suspensions of multilamellar vesicles of DMPC/DMPS (dimyristoylphosphatidylcholine/dimyristoylphosphatidylserine) (3:1; −•−), and in homogeneous media (ethanol; −). Molar proportions of *t*-PnA/*x* were 1:3 (x = DPPC in multilayers), 1:9 (x = AA in multilayers), and 1:500 (x = DPPC in vesicles). Concentration of *t*-PnA in ethanol = 7.24×10^{-6} M.

TABLE 2: Second and Fourth Rank Order Parameters for the Systems Studied[a]

description	$\langle P_2 \rangle$	$\langle P_4 \rangle$	λ_2	λ_4	remark
DPPC/*t*-PnA (3:1)	0.79	0.7	1.3592	4.183	$r = 0.34$; $w = 0.60$
AA/*t*-PnA (9:1)	0.72	0.72	0.3869	5.5934	$r = 0.34$; $w = 0.69$
DPPC/*t*-PnA	0.64	0.24	3.9042	−0.5758	liquid-crystal phase, BD simulation

[a] λ_2 and λ_4 are Lagrange multipliers that result from the application of the maximum entropy method to obtain the orientational distribution functions.

Namely, the spectral shift observed when the fatty acid is used remarkably agrees with the calibration plot (transition energy vs $(n_0^2 - 1)/(n_0^2 + 2)$, where n_0 is the refractive index of the medium), carried out by Sklar et al.[19] The slightly distorted vibrational progression of *t*-PnA in LB films of DPPC may result from exciton interaction due to the high molar fraction of this fatty acid in the system (25%).

The extremely low values of $A_{\omega=\pi/2}$ (results not shown) are a clear indication that the chromophore transition moment is almost perpendicular to the plane of the bilayer. Calculations of $\langle P_2 \rangle$ from the dichroic ratios in the UV−vis absorption experiments and $\langle P_4 \rangle$ from steady-state fluorescence measurements further confirm this result (Table 2). Because the transition moment of *t*-PnA is almost parallel to the molecular axis,[4] this means that the fatty acid molecules (at least its chromophore) are very orderly aligned with the host matrix, even in the case when DPPC is used. Studies of fatty acid/phospholipid interactions are rather scarce, although of biological relevance.[20,21] These results are, to our best knowledge, the first on the orientational order of a fatty acid in a lipidic bilayer, with a completely experimental approach, including $\langle P_2 \rangle$ and $\langle P_4 \rangle$.

The single particle orientation distributions $f(\psi)$ (Figure 6A) were calculated as outlined above. The maximum obtained for the experimental systems (AA and gel-phase DPPC) lie at 0° and are narrow. *t*-PnA is highly ordered in these systems, perpendicular to the plane of the multilayers. These results show that *t*-PnA incorporated in gel-phase DPPC is itself under conformational constraints which are typical from gel phases. This observation is in agreement with reported values for the partition coefficient of *t*-PnA in biphasic-gel/liquid-crystal lipidic

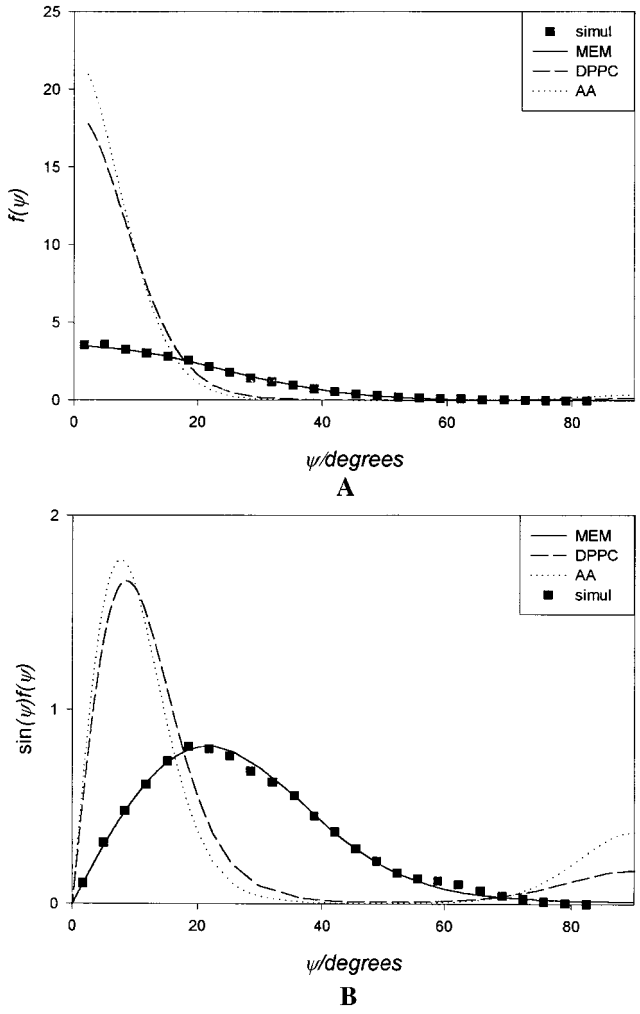

Figure 6. Orientation distribution functions (A) and probability density functions (B) for *t*-PnA in AA (···) and DPPC (− −) multilayers at room temperature. The data for BD simulations of *t*-PnA in a liquid-crystalline phase of DPPC (■), as well as the corresponding function, obtained from the maximum entropy method (−), is also presented.

environments,[3] which show a preference for gel phases. This preference is quite uncommon among lipidic probes.

The function $\sin(\psi)\ f(\psi)$ has a more direct physical meaning than $f(\psi)$ because it is the orientation probability density function. Figure 6B shows that $\sin(\psi)\ f(\psi)$ peaks at $\psi \approx 8°$ and $\langle\psi\rangle \approx 12°$ for both AA and gel-phase DPPC. Although it is intuitive to relate these values with the host matrix chain tilts, a quantitative comparison is not obvious and is model-dependent.[22] Whereas chain tilts in AA and gel-phase DPPC are expected to be 20−30°[23] and 19°,[24] respectively, the angles reported for linear free probes are typically smaller (e.g., 1,6-diphenylhexatriene (DPH[6])). It is worth mention that the reported distributions for DPH are also bimodal,[25] and this increased complexity of the system further hampers a quantitative relationship between the probe orientation and host chain tilt. Nevertheless, a bimodal (two-population) distribution for *t*-PnA is not a safe conclusion to be withdrawn from data in Figure 6B. The relative area of the peaks at $\psi = 90°$ is small, and a spurious nature cannot be discarded. Numerical artifacts may result from maximum entropy method application with only two terms, $\langle P_2\rangle$ and $\langle P_4\rangle$ (eq 5). Relatively small differences in the ($\langle P_2\rangle$, $\langle P_4\rangle$) pair may, in some cases, result in turning unimodal distributions into slightly bimodal ones.[26] A bimodal distribution may also result from a small fraction of molecules with deficient deposition.

The $\sin(\psi)\ f(\psi)$ experimental distributions (Figure 6B) are narrow. This result only occurs in a cylindrical molecule when both the molecular axis and the transition moment are collinear (or very close to it) and a very restricted molecular orientational freedom exists.

Multilayers of liquid-crystal DPPC deposited over quartz are not possible to achieve experimentally by the LB technique. So, we have performed BD simulations as an alternative approach because it is a quite powerful tested methodology.[27] $\langle P_2\rangle$ and $\langle P_4\rangle$ values calculated directly from the simulated trajectories are in Table 2. In BD simulations, ψ is the angle formed by the imaginary vector that joins C_9 and C_{16} (extremity elements that form the fluorescent entity of *t*-PnA) and the bilayer normal. The $f(\psi)$ function obtained from this pair of values using the maximum entropy method (eq 5) is depicted in Figure 6A, along with the orientational data collected directly from the trajectories. A good agreement is obtained, confirming that the methodology used for the calculation of $f(\psi)$ is adequate. The distribution is clearly shifted toward higher angles and is broader, in agreement with data on the dynamics of the system.[3] Because the molecular axis and transition moment are nearly collinear, the broad distribution width can safely be attributed to molecular orientational freedom.

BD simulations provide an easy way to analyze a large number of systems subject to various conditions such as molecular composition, bilayer thickness, temperature, and many more.[14,28,29] Detailed and reliable information about conformational and dynamical properties of acyl-like chains is provided by BD simulations.[14,29] The mean field potentials used in our simulations have thoroughly proved their suitability[14,28] and can be used to provide very important information.

Concerning simulation studies of unsaturated chain probes, the most relevant reported data deals with molecules in an isotropic medium[11] and also in a lipidic bilayer environment.[29] The simulation by BD with atomic level detail of a membrane probe in order to recover specific properties is rather new. We performed BD simulations to recover the *t*-PnA chromophore angular distribution inserted in a DPPC bilayer in the liquid-crystal phase. We did so because of the inaccessibility of experimental techniques to determine the angular distribution in the reported conditions. This approach, with its outcome, enhances the importance of computer simulations with predictive behavior and shows the benefits resulting from the intersection of experimental and simulation fields.

Conclusions

The transition moment of *t*-PnA is almost perpendicular to the plane of the DPPC or AA layers at room temperature. This result is in agreement with chemical intuition but had never been proven before. Because the transition moment is practically collinear to the molecular axis, a parallel arrangement of the *t*-PnA molecules with the host molecular matrix (gel-phase DPPC or AA) can be concluded. Moreover, the orientation density probability function is quite narrow. These results show that *t*-PnA is in a highly ordered, gel-like condition. This enlightens the preference of this probe for gel domains in multiphasic systems, which is one of the most intriguing properties of this polyene molecule.

BD simulations of *t*-PnA in liquid-crystal DPPC bilayers reveal that upon the main thermotropic phase transition of DPPC the orientational distribution is shifted toward higher angles relative to the multilayer normal and is broader. Besides the conclusions regarding *t*-PnA itself, this work shows that BD simulations of unsaturated acyl chains are possible, reliable, and simple with the mean field potentials reported here.

Acknowledgment. We thank Fundação para a Ciência e Tecnologia (Portugal) for Grant PRAXIS XXI BD/9393/96 to M.X.F. and funding (Project PRAXIS XXI/P/SAU/14025/1998).

References and Notes

(1) Hudson, B. S.; Cavalier, S. A. *Studies of membrane dynamics and lipid−protein interactions with parinaric acid*; Loew, L. M., Ed.; CRC Press: Boca Raton, FL, 1988; Vol. 1.
(2) Sklar, L. A.; Hudson, B. S.; Simoni, D. *Biochemistry* **1977**, *16*, 819.
(3) Mateo, C. R.; Brochon, J.-C.; Lillo, M. P.; Acuña, A. U. *Biophys. J.* **1993**, *65*, 2237.
(4) Shang, Q.; Hudson, B. S.; Dou, X. *Nature* **1991**, *352*, 703.
(5) Roberts, G. G., Ed.; *Langmuir−Blodgett films*; Plenum Press: New York, 1990.
(6) Krishma, M. M. G.; Periasamy, N. *J. Fluoresc.* **1998**, *8*, 81.
(7) Kooyman, R. P. H.; Levine, Y. K.; Van der Meer, B. W. *Chem. Phys.* **1981**, *60*, 317.
(8) Pottel, H.; Herreman, W.; Van der Meer, B. W.; Ameloot, M. *Chem. Phys.* **1986**, *102*, 37.
(9) Johansson, L.; Valmark, T.; Lidblom, G. *J. Chem. Soc., Faraday Trans. 1* **1985**, *81*, 1389.
(10) Wolber, P. K.; Hudson, B. S. *Biochemistry* **1981**, *20*, 2800.
(11) Rey, A.; Kolinski, A.; Skolnock, J.; Levine, Y. K. *J. Chem. Phys*. **1992**, *97*, 1240.
(12) Ryckaert, J. P.; Bellemans, A. *Chem. Phys. Lett.* **1975**, *30*, 123.
(13) Huertas, M. L.; Cruz, V.; López Cascales, J. J.; Acuña, A. U.; García de la Torre, J. *Biophys. J.* **1996**, *71*, 1428.
(14) Fernandes, M. X.; Huertas, M. L.; Castanho, M. A. R. B.; García de la Torre, J. *Biochim. Biophys. Acta* **2000**, *1463*, 131.
(15) Wiener, M. C.; White, S. H. *Biophys. J.* **1992**, *61*, 434.
(16) Seelig, A.; Seelig, J. *Biochemistry* **1974**, *13*, 4839−4845.
(17) Ermak, D. L.; McCammon, J. A. *J. Chem. Phys*. **1978**, *69*, 1352.
(18) Iniesta, A.; García de la Torre, J. *J. Chem. Phys*. **1990**, 92, 2015.
(19) Sklar, L. A.; Hudson, B. S.; Peterson, M.; Diamond, J. *Biochemistry* **1977**, *16*, 813.
(20) Zhang, F.; Kamp, F.; Hamilton, J. A. *Biochemistry* **1996**, *35*, 16055.
(21) Kamp, F.; Hamilton, J. A. *Biochemistry* **1993**, *32*, 11074.
(22) Krishna, M. M. G.; Periasamy, N. *Chem. Phys. Lett.* **1998**, *298*, 354.
(23) Tristam-Nagle, S.; Zhang, R.; Suter, R. M.; Worthington, C. R.; Sun, W.-J.; Nagle, J. F. *Biophys. J.* **1993**, *64*, 1097.
(24) Hasegawa, T.; Ushiroda, Y.; Kawaguchi, M.; Kitazawa, Y.; Nishiyama, M.; Hiraoka, A.; Nishijo, J. *Langmuir* **1996**, *12*, 1566.
(25) Van der Heide, U. A.; van Grinkel, G.; Levine, Y. K. *Chem. Phys. Lett.* **1996**, *253*, 118. Yang, J.; Kleijn, J. M. *Biophys. J.* **1999**, *76*, 323.
(26) Bos, M. A.; Kleijn, J. M. *Biophys. J.* **1995**, *68*, 2566.
(27) Gardinier, C. W. *Handbook of stochastic methods for physics, chemistry and natural sciences*; Springer: Berlin, Germany, 1983.
(28) Fernandes, M. X.; Huertas, M. L.; Castanho, M. A. R. B.; García de la Torre, J. *Biophys. Chem.* **1999**, *79*, 41.
(29) Pearce, L. L.; Harvey, S. C. *Biophys. J.* **1993**, *65*, 1084.
(30) Lamm, G.; Szabo, A. *J. Chem. Phys.* **1986**, *85*, 7334.